The Seismic Sequence of the 16 September 2015 M_w 8.3 Illapel, Chile, Earthquake

by Sergio Ruiz, Emilie Klein, Francisco del Campo, Efrain Rivera, Piero Poli, Marianne Metois, Vigny Christophe, Juan Carlos Baez, Gabriel Vargas, Felipe Leyton, Raúl Madariaga, and Luce Fleitout

ABSTRACT

On 16 September 2015, the M_w 8.3 Illapel, Chile, earthquake broke a large area of the Coquimbo region of north-central Chile. This area was well surveyed by more than 15 high-rate Global Positioning System (GPS) instruments, installed starting in 2004, and by the new national seismological network deployed in Chile. Previous studies had shown that the Coquimbo region near Illapel was coupled to about 60%. After the M_w 8.8 Maule megathrust earthquake of 27 February 2010, we observed a large-scale postseismic deformation, which resulted in a strain rate increase of about 15% in the region of Illapel. This observation agrees with our modeling of viscous relaxation after the Maule earthquake. The area where upper-plate GPS velocity increased coincides very well with the slip distribution of the Illapel earthquake inverted from GPS measurements of coseismic displacement. The mainshock started with a small-amplitude nucleation phase that lasted 20 s. Backprojection of seismograms recorded in North America confirms the extent of the rupture, determined from local observations, and indicates a strong directivity from deeper to shallower rupture areas. The coseismic displacement shows an elliptical slip distribution of about 200 km × 100 km with a localized zone where the rupture is deeper near 31.3° S. This distribution is consistent with the uplift observed in some GPS sites and inferred from field observations of bleached coralline algae in the Illapel coastal area. Most of aftershocks relocated in this study were interplate events, although some of the events deeper than 50 km occurred inside the Nazca plate and had tension (slab-pull) mechanisms. The majority of the aftershocks were located outside the 5 m contour line of the inferred slip distribution of the mainshock.

Online Material: Catalog of relocated seismicity.

INTRODUCTION

At 22:54:31 (UTC) on 16 September 2015, an M_w 8.3 earthquake occurred near the city of Illapel in the Coquimbo region of north-central Chile. Using all available local data, we located this event at 71.7° W, 31.5° S, in agreement with the location from the Centro Sismológico Nacional (CSN) of the Universidad de Chile, Chile. The event broke a well-instrumented area, with more than 15 high-rate GPS instruments deployed between 2004 and 2007 (Vigny *et al.*, 2009) and several broadband and strong-motion instruments deployed by CSN (Fig. 1). Coupling models computed from GPS data identified an extended area (from 34° S to 30.5° S) between the Nazca and South American plates where coupling was higher than 60% (Métois *et al.*, 2014, 2016). The Illapel earthquake occurred between two lower coupling zones (LCZs): a small zone near 32° S, and a larger one in the north, near 30.5° S in front of La Serena. These LCZs coincide with two major oceanic structures of the Nazca plate that are currently colliding with the continental South American plate: the Challenger fracture zone and the Juan Fernandez Ridge (Fig. 2).

The Illapel earthquake occurred near the northern end of the rupture zone of the 1730 mega-earthquake (Montessus de Ballore, 1912, Urrutia and Lanza, 1993; Lomnitz, 2004; Udías *et al.*, 2012), a large megathrust earthquake ($M_w \sim 9.0$) that probably controls the seismic cycle of central Chile (see Fig. 2). A recent paleoseismological study (Dura *et al.*, 2015) proposes a recurrence interval between ~200 and ~650 years for these mega-earthquakes. Considering two earthquakes of magnitude $M_w \sim 8.0$ occurred previously (in 1943 and 1880; Beck *et al.*, 1998), Nishenko (1985) suggested that the Illapel zone was a seismic gap. Several other large events occurred in the last century south of the Illapel rupture: Valparaiso in 1906 (M_w 8.6), La Ligua in 1971 (M_w 7.9), Valparaíso in 1985 (M_w 8.0), and Maule in 2010 (M_w 8.8) (Malgrange *et al.*, 1981; Comte *et al.*, 1986; Vigny *et al.*, 2011). The La Serena LCZ appears to be a barrier to seismic ruptures; for example, the 1922 Atacama megathrust earthquake stopped just to the north in this zone (Beck *et al.*, 1998) (Fig. 2).

Seismicity in the Coquimbo region increased in the last 15 years, after a swarm of several $M_w \sim 6.0$ events occurred in the plate interface in July–October 1997 (Fig. 3). These

doi: 10.1785/0220150281

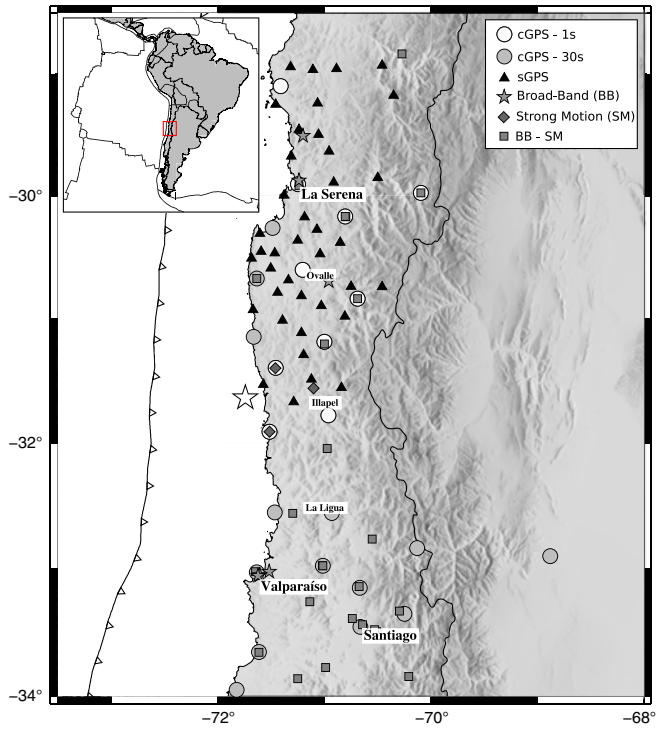

▲ **Figure 1.** Global Positioning System (GPS), Broadband (BB), and strong-motion (SM) stations in the Coquimbo–Valparaiso regions of central Chile. Continuous GPS (cGPS)-1 s stations record continuously in time at 1 Hz. cGPS-30 s stations record continuously in time every 30 s. sGPS are static survey stations. BB–SM stations are sites where a broadband and an accelerometer are installed, sampling at 100 Hz. SM are sites where strong-motion sensors are located, and BB are the temporary broadband stations deployed one day after of mainshock. The star marks the epicenter of the Illapel earthquake. The color version of this figure is available only in the electronic edition.

events preceded the 1997 M_w 7.1 Punitaqui intraplate compressional (slab-push) intermediate-depth earthquake of 15 October 1997 (Lemoine *et al.*, 2001; Pardo *et al.*, 2002; Gardi *et al.*, 2006). The sudden seismicity increase in 1997, together with the previous occurrence of the 1730 megathrust earthquake, encouraged the deployment of a GPS network in the Coquimbo region (Vigny *et al.*, 2009). Since 2004, a group of researchers of Institute de Physique du Globe de Paris and École Normale Supérieure, France, and Universidad de Chile deployed a GPS network that has been fully operational since 2007. This dense network and the broadband and strong-motion instruments deployed by the CSN in recent years (Fig. 1) monitor the long- and short-term processes of upper-plate deformation. We supplemented the instrumental information with coseismic uplift observations of bleached lithothamnioids crustose coralline algae (Ortlieb *et al.*, 1996; Farías *et al.*, 2010; Vargas *et al.*, 2011) located in the coastal zone of Coquimbo region. In this study, we analyzed the earthquake sequence of the M_w 8.3 Illapel earthquake using the GPS time series, the coseismic rupture using local and teleseismic data, and the aftershock distribution using the local broadband data.

BEFORE THE 2015 ILLAPEL MAINSHOCK

The historical seismicity of Chile was compiled, among others, by Montessus de Ballore (1912), Urrutia and Lanza (1993), and Lomnitz (2004), who extended their work back to Spanish settlements in the middle of the sixteenth century. Central Chile seismicity, as was mentioned earlier, is dominated by the 1730 mega-earthquake (Lomnitz, 2004; Udías *et al.*, 2012), followed by several events of magnitude close to M_w 8.0 that occurred in the nineteenth and twentieth centuries (Fig. 2a). In the northern end of the zone (30.5° S) where the city of La Serena was established in 1544, the situation is quite different. There is little information about earthquake damage to buildings; only small tsunamis in 1730, 1849, 1880, and 1922 had been reported (Urrutia and Lanza, 1993)—and now again, following the Illapel 2015 event. Low coupling values deduced from GPS measurements of the upper-plate deformation around La Serena are consistent with these historical observations. In contrast, higher coupling is observed to the south of the 2015 Illapel rupture. The coupling map (Fig. 2c) shows indeed a striking segmentation at 32° S and 30° S. GPS measurements conducted during the interseismic period showed that only a small portion of the coast between 31.5° S and 31° S was subsiding, suggesting a deepening of the highly coupled zone (Métois *et al.*, 2014, 2016).

Similarly to what was observed before the 2011 Tohoku and 2014 Iquique earthquakes (Kato *et al.*, 2012; Ruiz *et al.*, 2014), transient deformation revealed by changing upper-plate velocities was observed in the Illapel zone prior to the seismic rupture. This transient deformation is observed in the continuous GPS (cGPS) time series of stations in the area where a significant change in velocity trend was observed after the 2010 Maule mega-earthquake (Fig. 4). A similar observation was made at campaign GPS sites that were measured about 10 times before 2010 and yearly since that time (Fig. 4b). According to Klein *et al.* (2016), this change in the velocity field was produced by postseismic viscoelastic relaxation due to the 2010 Maule earthquake. The relaxation took place mainly in the asthenosphere and in a thin viscous channel in the deep interface between the Nazca and South American plates, as expected from viscoelastic rebound modeling. As previously observed following giant megathrust earthquakes—for example, 1960 M_w 9.5 Valdivia (Khazaradze and Klotz, 2003), 2005 M_w 9.2 Sumatra (Hu and Wang, 2012), and 2011 M_w 9.1 Tohoku (Watanabe *et al.*, 2014) earthquakes—post-Maule upper-plate velocities show sustained trench-ward displacements in front of the rupture area. In the middle of the 2010, rupture zone postseismic deformation contributes significantly to the release of strain in the upper plate. On the other hand, at both edges of the 2010 rupture, we observed a rotation of the postseismic displacements toward inland directions (Fig. 5). In the Illapel area,

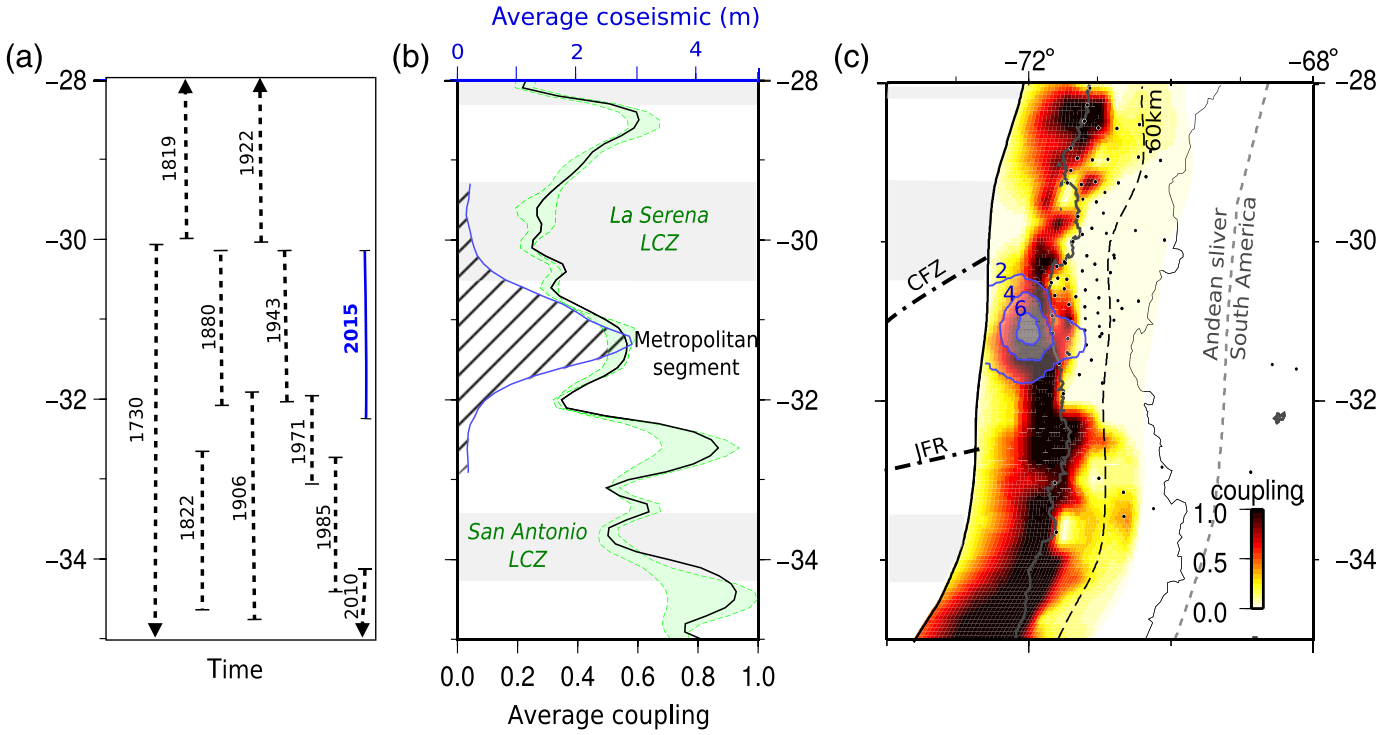

▲ **Figure 2.** (a) Lateral extent of historical ruptures inferred in central Chile (Urrutia and Lanza, 1993; Beck *et al.*, 1998; Lomnitz, 2004). (b) Along-strike variations of the average coupling value from the trench to 60 km depth and two alternative models that fit almost equally well with the data (different smoothing parameters, dashed curves). The average coseismic slip amount for the 2015 Illapel earthquake is the dashed area. Both interseismic averaged coupling and averaged coseismic slip curves have been calculated with 0.2°-wide sliding windows. The lower coupling zones (LCZs) are indicated (modified from Métois *et al.*, 2016). (c) Interseismic coupling distribution for central Chile: thin dashed line, 60-km-depth slab contour; dots, position of GPS stations used for the inversion; and contour curves, 2 m coseismic-slip contours for our proposed Illapel slip distribution. The Challenger fracture zone (CFZ) and Juan Fernandez Ridge (JFR) are indicated. The color version of this figure is available only in the electronic edition.

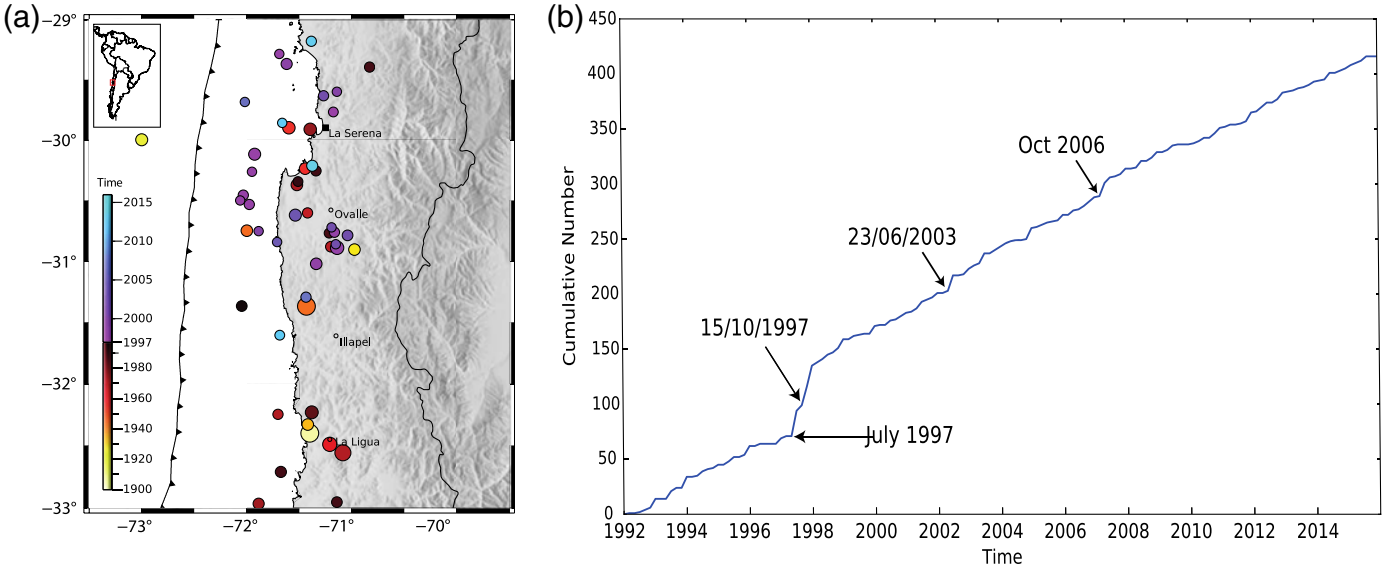

▲ **Figure 3.** (a) Seismicity larger than magnitude M_w 6.0 that preceded the main event of 16 September 2015. (b) Cumulative seismicity versus time. The slope of the curve is proportional to the rate of the seismicity of magnitude larger than M_w 4.5 from National Earthquake Information Center (NEIC) catalog. The color version of this figure is available only in the electronic edition.

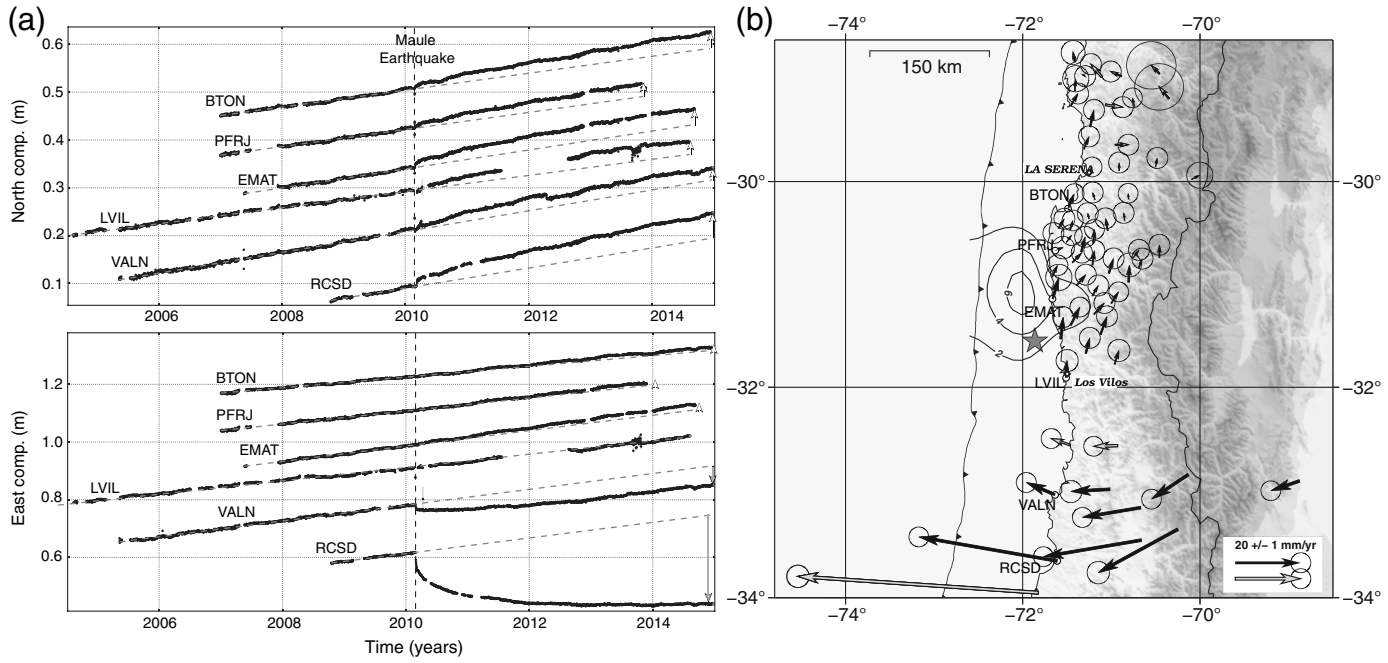

▲ **Figure 4.** (a) Time series of coastal GPS permanent stations, ordered by increasing latitude, for the north (top) and the east (bottom) components (comp.). The dotted lines represent the preseismic trends estimated before the Maule earthquake, open arrows highlight the postseismic increase of the trend. (b) Residual velocities (difference between the postseismic [post-2010] and the preseismic [pre-2010] velocities) in mm/yr. cGPS stations represented in (a) are identified by their names and dots. Gray vectors represent less-well-known velocities (few campaign measurements or interpolated pre-2010 velocities). The slip distribution is roughly represented by its contour lines. The star shows the epicenter.

this yields northeastern directions, roughly aligned with the preseismic directions, producing an increase close to 15% of upper-plate GPS velocities and thus leading to an increase of strain accumulation in the upper plate.

THE COSEISMIC RUPTURE PROCESS OF THE m_W 8.3 ILLAPEL EARTHQUAKE

In spite of the increase in the upper-plate strain rate that we detected during the five years before the Illapel earthquake, we did not observe any significant increase in the seismicity of the area during the weeks before the mainshock. The coseismic rupture process of the 2015 M_w 8.3 Illapel event started with a relatively weak amplitude phase (or immediate foreshock) that had a strong south to north directivity, as can be observed in the near-field records and in the backprojection results (Fig. 6).

Direct imaging of the M_w 8.3 Illapel earthquake was obtained by backprojection of teleseismic *P*-waves. For this purpose, we used the *P*-waves recorded at the Transportable Array network (Meltzer *et al.*, 1999). After deconvolution of the instrument response, the velocity seismograms were filtered between 0.2 and 1 Hz and aligned according to the theoretical *P*-wave travel time predicted by the IASP91 model (Kennett, 1991). To account for 3D velocity anomalies along the *P*-wavepath into the mantle, we further aligned the traces using an iterative procedure based on multichannel correlation technique (VanDecar and Crosson, 1990). The delay and polarity of each channel were updated during each iteration. Only *P*-waves with correlation coefficient larger than 0.8 were retained for the stack. The first arrival is assumed to come from our proposed epicenter (71.7° W, 31.5° S), whereas the timing

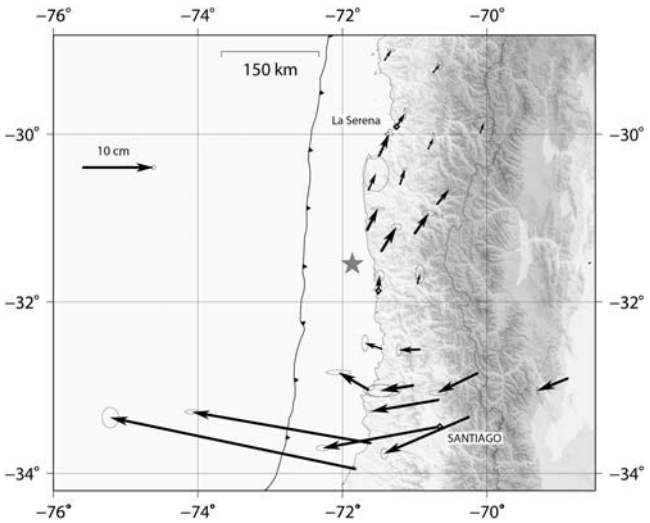

▲ **Figure 5.** Horizontal cumulative displacements (in centimeters) over five years (between 2010 and the end of 2014), corrected from interseismic trends (modified from Klein *et al.*, 2016).

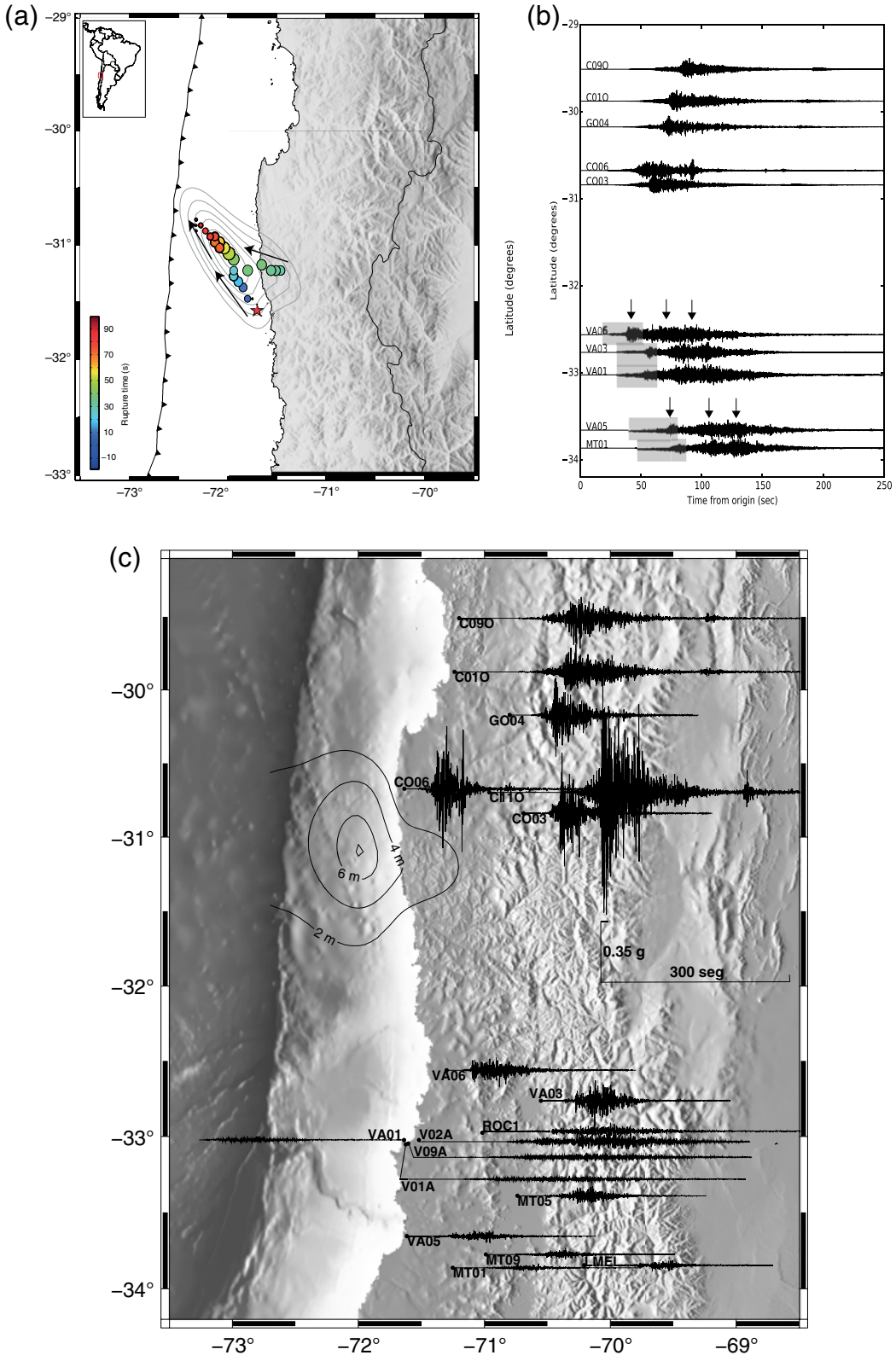

▲ **Figure 6.** (a) Backprojection of the 2015 Illapel mainshock. The dots represent the locations of the sources determined from backprojection of teleseismic *P*-waves and are coded following the rupture time measured with respect to the hypocentral time. (b) Strong-motion records (east–west components) ordered by latitude: the arrows show the arrivals of different bursts of energy, and the gray rectangles show the seismic waves associated with the first starting phase. (c) Strong-motion records (east–west components) of the M_w 8.3 Illapel earthquake recorded by the Centro Sismológico Nacional (CSN). The color version of this figure is available only in the electronic edition.

of each ensuing coherent arrival is obtained by stacking the seismograms after calculating the differential travel time from each potential source to the hypocenter. The source area was discretized with a grid with spacing of 0.1°. To enhance the coherence of the later arrival, a four-root stacking procedure was applied (Koper *et al.*, 2011).

Figure 6 shows that the strong ground motions recorded at stations located south of the epicenter have longer durations than those situated to the north. Also, in the southern records, we observed three distinct pulses that are not clearly identified in the northern records. We attributed this difference to strong northward directivity. The first large amplitude accelerations observed in the strong-motion records (shaded zone in Fig. 6b) correspond to the initial rupture. We estimated the seismic moment of the immediate precursor as M_o 2.61×10^{19} N·m, equivalent to M_w 6.9; which is a small fraction of the M_o 3.94×10^{21} N·m (M_w 8.3) obtained from GPS data for the coseismic displacement for the main event (Fig. 7a).

Assuming that the fault surface was situated at the plate interface as defined by Hayes *et al.* (2012), the slip distribution for the Illapel earthquake was inverted from GPS data. The fault surface was discretized into many rectangles of 100 km^2. The lithosphere was approximated as linear elastic, homogeneous, and isotropic half-space. The displacement at any observation point is calculated using the formulation of Okada (1985). Our resolution was verified by a checkerboard test (Fig. 7b) with patches of 60 km × 60 km. At this scale, there is a good resolution near the coast except south of 32.5° S but very little resolution close to the trench and below 60 km of depth. Our results show that, between 31° S and 31.5° S, the rupture is located in a narrow deep contact zone coinciding with the observed coseismic coastal uplift zone that was previously subsiding during the interseismic period (Fig. 8).

Along the coast of the epicentral area, we observed a conspicuous white fringe of bleached lithothamnioids crustose coralline algae that, together with dry littoral communities, confirmed the coseismic coastal uplift (Fig. 8). In particular, bleached lithothamnioids have been used as a marker of rapid vertical coseismic displacements during field surveys following other recent earthquakes along the Chilean subduction margin, such as the M_w 8.0 Antofagasta earthquake in 1995 (Ortlieb *et al.*, 1996) and the M_w 8.8 Maule earthquake in 2010 (Farías *et al.*, 2010; Vargas *et al.*, 2011). These algae can be found attached to the rocks between the subtidal and the lower intertidal zones. The most obvious lithothamnioids algae recognizable in the field are of reddish–pinkish color (Guiler, 1959) and turn white when suddenly exposed to solar radiation with no permanent humidification, possibly because of calcareous secretions (Ortlieb *et al.*, 1996; Vargas *et al.*, 2011). For the Illapel earthquake, we especially observed these bleached algae at Puerto Oscuro, just in front of the epicenter (Fig. 8b), and along the coast located immediately to the north (Fig. 8c).

AFTERSHOCKS

The CSN catalog for the Coquimbo region is complete starting from local magnitude $M_L \sim 4.0$ since the installation of the new seismic network in 2014. This catalog shows that the aftershock zone extended from 29° S to 33° S two weeks after the main event (Fig. 9). Figure 9 shows that the rupture of the Illapel earthquake was followed by a large zone of aftershocks that surrounds the 5 m contour line of the coseismic slip distribution.

We used local data to relocate and compute the centroid depth of the moment tensor for the aftershocks (Fig. 10). We located the precursory seismicity using the SEISAN software (Havskov and Ottemöller, 1999) with the same velocity model used by CSN for this zone (Tables 1 and Ⓔ S1, available in the electronic supplement to this article). We relocated 78 events of magnitudes larger than M_w 5.0 that occurred from 16 September 2015 to 5 October 2015. The CSN catalog was used as reference. The events were relocated using the arrival time of *P* and *S* waves hand-picked from all available traces with a visually good signal-to-noise ratio. Once the aftershocks were relocated, the centroid moment tensor for 51 events was computed using the Computer Programs in Seismology package (Herrmann, 2013). For this purpose, the epicenter location was fixed while we searched for the centroid depth and the best-fitting double-couple source mechanism. This was done by a grid search: for each possible depth, we tested all possible double couples and kept those that minimized the variance between observed and simulated traces. Figure 10 shows that aftershocks mostly occurred outside the 5 m contour line of the slip distribution, consistent with previous observations of anticorrelations between mainshock slip and aftershock distributions (Das and Henry, 2003; León-Ríos *et al.*, 2016). The aftershocks are located in the deeper zone of the contact beyond 50 km from the trench, just like those following the 2007 Tocopilla and 2010 Maule earthquakes (Agurto *et al.*, 2012; Fuenzalida *et al.*, 2013). This aftershock distribution is different from that of the 2014 Iquique earthquake, in which the aftershocks were mainly located in the upper plate, below the accretionary wedge (León-Ríos *et al.*, 2016) (Fig. 10). Another interesting feature of this sequence is that several small events reported by CSN are outer rise, whereas other events are intraplate intermediate depth, similar to the 1997 M_w 7.1 Punitaqui earthquake.

DISCUSSION AND CONCLUSIONS

As shown in Figure 3, before the Illapel earthquake, we observed a steady increase in seismicity in the Coquimbo region that started right after the occurrence of the Punitaqui intermediate-depth earthquake on 15 October 1997. In the period from the end of 1997 until the Illapel earthquake in September 2015, several events clustered in time (Vigny *et al.*, 2009). However, in the weeks before the Illapel earthquake of 16 September 2015, we did not observe any particular seismicity increase, in contrast to what we observed before the

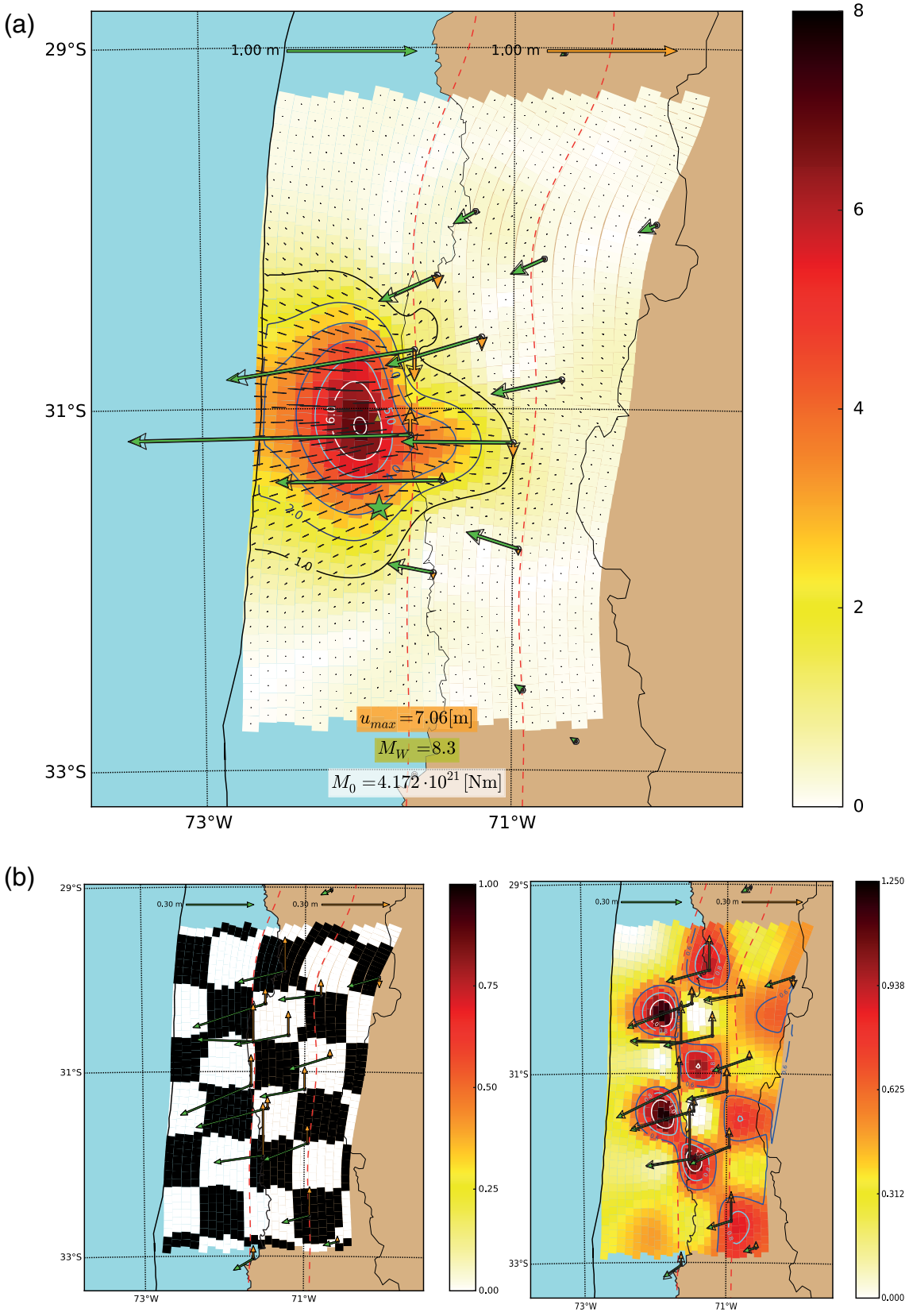

▲ **Figure 7.** Slip distribution of the 2015 Illapel earthquake. (a) Coseismic slip distribution inverted from static GPS displacements (difference between 17 September and 16 September) showing the discretization used in this work. (b) Checkerboard test for the finite source slip inversion using squares of 60 km of side (left figure, input model; right figure, recovered model). The color version of this figure is available only in the electronic edition.

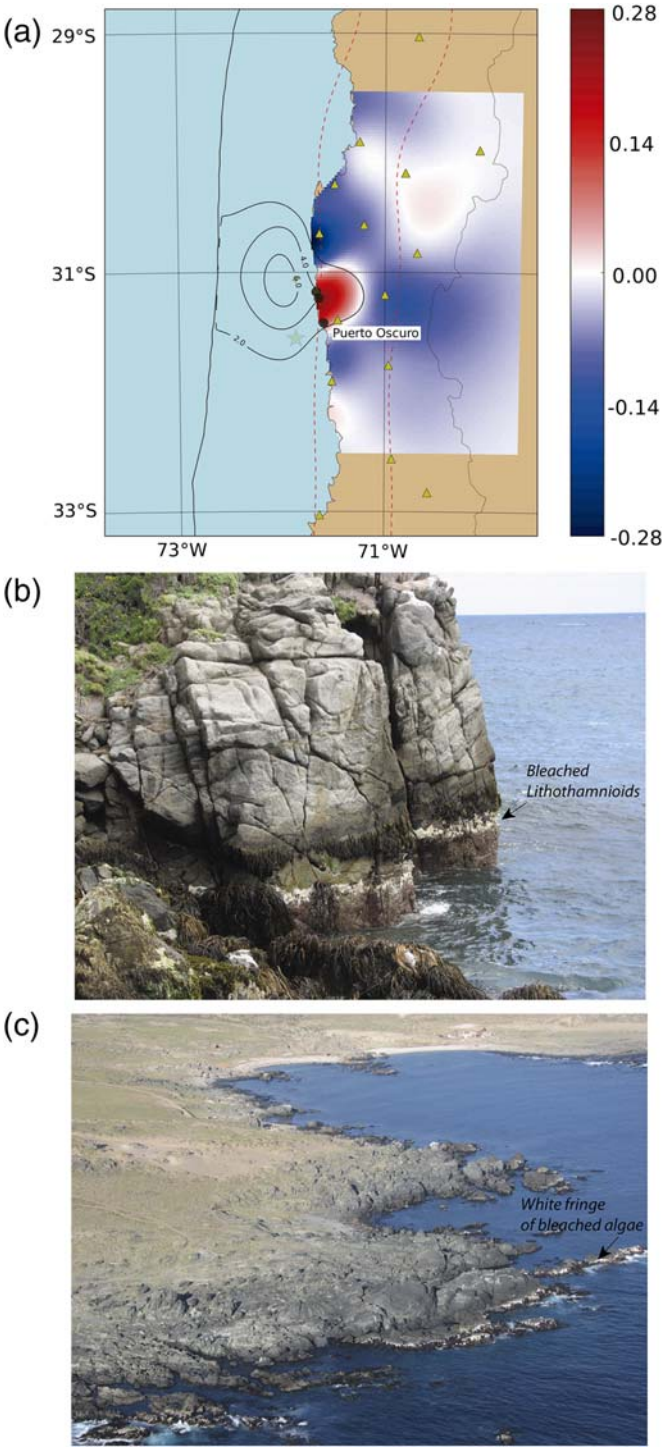

▲ **Figure 8.** Vertical uplift produced by the 2015 Illapel earthquake. (a) Vertical displacements on the surface predicted by our coseismic slip distribution. Black dots are geological observation of coastal uplift; the triangles are locations of GPS antennas. (b) White fringe of bleached lithothamnioids observed at Puerto Oscuro, in front of the epicenter. (c) Aerial view of white fringe of bleached algae observed along the coast to the north of the epicenter. The color version of this figure is available only in the electronic edition.

2014 Iquique earthquake (Kato *et al.*, 2012; Ruiz *et al.*, 2014). On the other hand, after the 2010 M_w 8.8 Maule earthquake, an important increase (of up to 15%) of velocities derived from GPS measurements were observed at all stations located in the Illapel earthquake area (Klein *et al.*, 2016). We hypothesize that a possible reason for the triggering of the Illapel earthquake was that the viscoelastic deformation of the asthenosphere after the 2010 mega-earthquake induced a deep transient slow slip that changed the stress conditions in the seismogenic contact of this region. In contrast, south of 32° S, the deep viscoelastic relaxation produced an overall decrease of the velocities of the upper plate. The influence of viscoelastic deformation plus the presence of a low coupling boundary at −32°S and −30°S could have favored the occurrence of the Illapel earthquake, a large but frequent event of M_w 8.3 similar to the previous 1880 or 1943 events. The Illapel event may have delayed the triggering of an M_w 9 mega-earthquake, which would have been a repetition of the 1730 event.

The Illapel mainshock had a nucleation phase of about 20 s with a magnitude of around M_w 6.9. This initial phase has a strong south-to-north directivity observed in the teleseismic *P* waves of the Transportable Array of North America and in the local strong-motion records. Our inversion of coseismic displacement vectors shows an elliptical slip distribution of about 200 km × 100 km, with a narrow zone where the rupture is deeper between 31.5° S and 31° S. This is consistent with the uplift observed in the GPS sites and also inferred by our geological observations.

We relocalized 78 aftershocks and estimated the moment tensor of 51 of them. Most of these events are concentrated in the deeper parts of the plate interface. Near the trench, we did not observe large magnitude aftershocks, suggesting that the eroded and fractured volcanic wedge (Contreras-Reyes *et al.*, 2015) could be an up-dip limit of the seismic rupture. The fault-plane solutions for the aftershocks reveal mainly reverse faulting, showing a predominance of interplate events. Several events have along-slab tensional mechanisms (slab-pull) and are located near the top of the Nazca plate, at depths larger than 50 km. Finally, we observed that most of the aftershocks are located outside the 5 m contour line of the slip distribution that we inverted from GPS data for the 2015 Illapel earthquake.

DATA AND RESOURCES

Local data used in this study were collected by the National Seismological Center. Local seismic data can be accessed at http://evt.csn.uchile.cl (last accessed March 2016) and Global Positioning System (GPS) data at http://www.csn.uchile.cl and https://www.lia-mb.net (last accessed March 2016). The teleseismic data were obtained from Incorporated Research Institutions for Seismology Data Management Center (http://ds.iris.edu/wilber3, last accessed March 2016).

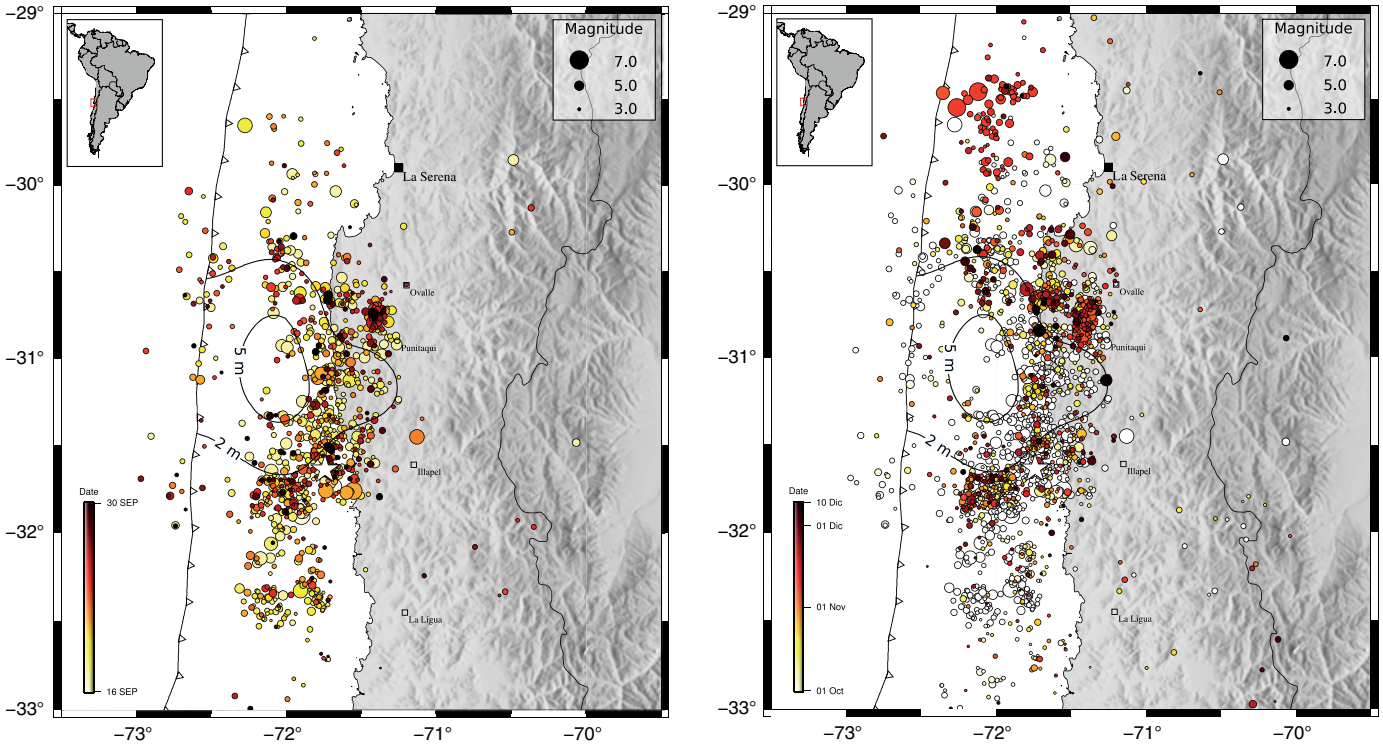

▲ **Figure 9.** Aftershocks of the 2015 Illapel earthquake. (a) Seismicity reported by CSN between 16 September 2015 and 30 September 2015. (b) Seismicity reported from CSN between 1 October 2015 and 10 December 2015. The open circles correspond to the seismicity shown in (a). Contours of the coseismic slip distribution of Figure 7 are plotted in the figures for reference. The color version of this figure is available only in the electronic edition.

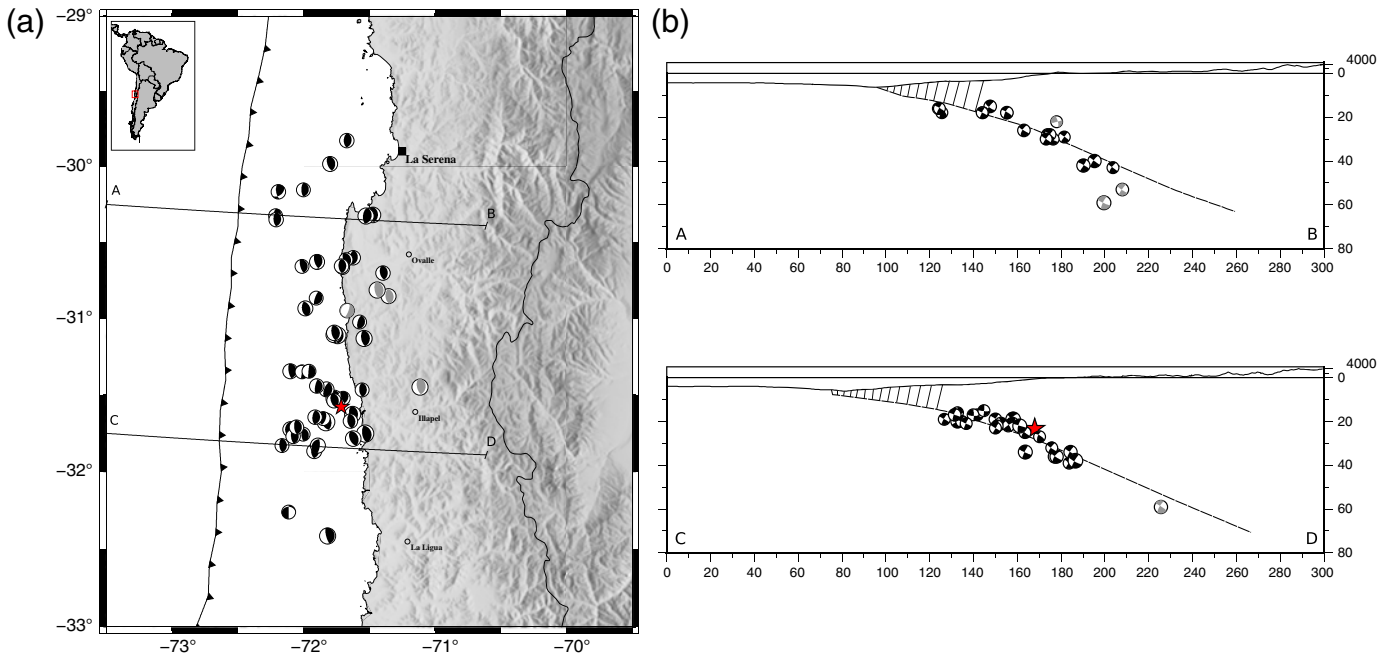

▲ **Figure 10.** Moment tensors of aftershocks of the 2015 Illapel earthquakes. (a) Moment tensor determination for events of magnitude greater than M_w 5.0 occurred between 16 September 2015 and 5 October 2015. The gray focal mechanisms are those interpreted as intraplate intermediate depth or crustal events. (b) Schematic profile of the Nazca plate subduction in the Illapel region based on Hayes *et al.* (2012) and Contreras-Reyes *et al.* (2015). The hatched zone is composed of eroded and fractured volcanics (Contreras-Reyes *et al.*, 2015) that could act as an up-dip limit for the seismic rupture. The color version of this figure is available only in the electronic edition.

Table 1
Velocity Model Used to Localize and Compute Moment Tensors Used in This Work and Used by the Centro Sismológico Nacional for This Zone

Depth (km)	V_P (km/s)
−5.00	5.079
5.00	5.910
10.00	5.929
15.00	6.790
20.00	6.960
25.00	6.961
30.00	6.962
35.00	7.129
40.00	7.340
45.00	7.620
50.00	7.920
55.00	7.961
60.00	8.194
70.00	8.195
80.00	8.220
100.00	8.429
120.00	8.440
150.00	8.441

ACKNOWLEDGMENTS

S. R. acknowledges the support of the Chilean National Science Foundation (NSF) project FONDECYT Number 11130230; R. M. acknowledges FONDECYT Number 1130636; and P. P. acknowledges NSF Grant Number EAR-1521534. We thank the Chilean Army for aerial recognition and J. Gonzalez and A. Villalobos for field support. We thank the Incorporated Research Institutions for Seismology Data Management Center, Centro Sismológico Nacional, and Montessus de Ballore Associated International Laboratory for making raw data available to us. Finally, we thank Zhigang Peng, Susan Hough, and one anonymous referee for their very useful and constructive reviews.

REFERENCES

Agurto, H., A. Rietbrock, I. Ryder, and M. Miller (2012). Seismic-afterslip characterization of the 2010 M_w 8.8 Maule, Chile, earthquake based on moment tensor inversion, *Geophys. Res. Lett.* **39,** L20303, doi: 10.1029/2012GL053434.

Beck, S., S. Barrientes, E. Kausel, and M. Reyes (1998). Source characteristics of historic earthquakes along the central Chile subduction zone, *J. South Am. Earth Sci.* **11,** 115–129.

Comte, D., A. Eisenberg, E. Lorca, M. Pardo, L. Ponce, R. Saragoni, S. K. Singh, and G. Suárez (1986). The 1985 central Chile earthquake: A repeat of previous great earthquake in the region? *Science* **233,** 449–453.

Contreras-Reyes, E., J. Ruiz, J. Becerra, H. Kopp, C. Reichert, A. Makysymowicz, and C. Arriagada (2015). Structure and tectonics of the central Chilean margin (31°–33° S): Implications for subduction erosion and shallow crustal seismicity, *Geophys. J. Int.* **203,** 776–791.

Das, S., and C. Henry (2003). Spatial relation between main earthquake slip and its aftershock distribution, *Rev. Geophys.* **41,** 1013, doi: 10.1029/2002RG000119.

Dura, T., M. Cisternas, B. Horton, L. Ely, A. Nelson, R. Wesson, and J. Pilarczyk (2015). Coastal evidence for Holocene subduction-zone earthquakes and tsunamis in central Chile, *Quarternary Sci. Rev.* **113,** 93–111.

Farías, M., G. Vargas, A. Tassara, S. Carretier, S. Baize, D. Melnick, and K. Bátanle (2010). Land-level changes produced by the M_w 8.8 2010 Chilean earthquake, *Science* **329,** no. 5994, 916, doi: 10.1126/Science.1192094.

Fuenzalida, A., B. Schurr, M. Lancieri, M. Sobiesiak, and R. Madariaga (2013). High resolution relocation and mechanism of aftershocks of the 2007 Tocopilla (Chile) earthquake, *Geophys. J. Int.* **194,** 1216–1238.

Gardi, A., A. Lemoine, R. Madariaga, and J. Campos (2006). Modeling of stress transfer in the Coquimbo region of central Chile, *J. Geophys. Res.* **111,** no. B04307, doi: 10.1029/2004JB003440.

Guiler, E. R. (1959). Intertidal belt-forming species on the rocky coasts of northern Chile, *Pap. Proc. Roy. Soc. Tasmania* **93,** 33–57.

Havskov, J., and L. Ottemöller (1999). SEISAN earthquake analysis software, *Seismol. Res. Lett.* **70,** 532–534

Hayes, G., D. Wald, and R. L. Johnson (2012). Slab1.0: A three-dimensional model of global subduction zone geometries, *J. Geophys. Res.* **117,** no. B01302, doi: 10.1029/2011JB008524.

Herrmann, R. B. (2013). Computer Programs in Seismology: An evolving tool for instruction and research, *Seismol. Res. Lett.* **84,** 1081–1088.

Hu, Y., and K. Wang (2012). Spherical-Earth finite element model of short-term postseismic deformation following the 2004 Sumatra earthquake, *J. Geophys. Res.* **117,** no B05404, doi: 10.1029/2012JB009153.

Kato, A., H. Obara, T. Igarashi, H. Tsuruoka, S. Nakagawa, and N. Hirata (2012). Propagation of slow slip leading up to the 2011 M_w 9.0 Tohoku-Oki earthquake, *Science* **335,** 705–708.

Kennett, B. L. N. (Compiler and Editor) (1991). *IASPEI 1991 Seismological Tables*, Bibliotech, Canberra, Australia, 167 pp.

Khazaradze, G., and J. Klotz (2003). Short and long-term effects of GPS measured crustal deformation rates along the south-central Andes, *J. Geophys. Res.* **108,** no. B4, 1–13.

Klein, E., L. Fleitout, C. Vigny, and J. D. Garaud (2016). Afterslip and viscoelastic relaxation model inferred from the large scale postseismic deformation following the 2010 M_w 3 8, 8 Maule earthquake (Chile), *Geophys. J. Int.* **205,** no. 2, doi: 10.1093/gji/ggw086.

Koper, K., A. Huko, T. Lay, C. Ammon, and H. Kanamori (2011). Frequency-dependent rupture process of the 11 March 2011 M_w 9.0 Tohoku earthquake: Comparison of short-period P wave backprojection images and broadband seismic rupture models, *Earth Planets Space* **63,** 599–602.

Lemoine, A., J. Campos, and R. Madariaga (2001). Evidence for earthquake interaction in the Illapel Gap of central Chile, *Geophys. Res. Lett.* **28,** 2743–2746.

León-Ríos, S., S. Ruiz, A. Maksymowicz, F. Leyton, A. Fuenzalida, and R. Madariaga (2016). Diversity of the Iquique's foreshocks and aftershocks: A clue about the complex rupture process of a M_w 8.1 earthquake, *J. Seismol.* doi: 10.1007/s10950-016-9568-6.

Lomnitz, C. (2004). Major earthquakes of Chile: A historical survey, 1535-1960, *Seismol. Res. Lett.* **75,** 368–378.

Malgrange, M., A. Deschamps, and R. Madariaga (1981). Thrust and extensional faulting under the Chilean coast: 1965 and 1971 Aconcagua earthquakes, *Geophys. J. Roy. Astron. Soc.* **66,** 313–332.

Meltzer, A., R. Rudnick, R. Zeitler, A. Lavander, G. Humphreys, K. Karlstrom, G. Ekström, R. Carlson, T. Dixon, M. Gurnis, *et al.* (1999). The USArray initiative, *GSA Today* **9,** 8–10.

Métois, M., C. Vigny, and A. Socquet (2016). Interseismic coupling, megathrust earthquakes and seismic swarms along the Chilean

subduction zone, *Pure Appl. Geophys.* **117,** no. B3, doi: 10.1007/s00024-016-1280-5.
Métois, M., C. Vigny, A. Socquet, A. Delorme, S. Morvan, I. Ortega, and M. C. Valderas-Bermejo (2014). GPS-derived interseismic coupling on the subduction and seismic hazards in the Atacama region, Chile, *Geophys. J. Int.* **196,** no. 2, 644–655, doi: 10.1093/gji/ggt418.
Montessus de Ballore, F. (1912). Historia Sísmica de los Andes meridionales al sur del paralelo XVI, in *Anales de la Universidad de Chile*, Imprenta Cervantes, Santiago, Chile, 545–591.
Nishenko, S. P. (1985). Seismic potential for large and great interplate earthquakes along the Chilean and southern Peruvian margins of South America: A quantitative reappraisal, *J. Geophys. Res.* **90,** 3589–3615, doi: 10.1029/JB090iB05p03589.
Okada, Y. (1985). Surface deformation due to shear and tensile faults in a half-space, *Bull. Seismol. Soc. Am.* **75,** 1135–1154.
Ortlieb, L., S. Barrientos, and N. Guzmán (1996). Coseismic coastal uplift and coralline algae record in northern Chile: The 1995 Antofagasta earthquake case, *Quarternary Sci. Rev.* **15,** 949–960.
Pardo, M., D. Comte, T. Monfret, R. Boroschek, and M. Astroza (2002). The October 15, 1997 Punitaqui earthquake (M_w = 7.1): A destructive event within the subducting Nazca plate in central Chile, *Tectonophysics* **345,** 199–210.
Ruiz, S., M. Metois, A. Fuenzalida, J. Ruiz, F. Leyton, R. Grandin, C. Vigny, R. Madariaga, and J. Campos (2014). Intense foreshocks and a slow slip event preceded the 2014 Iquique M_w 8.1 earthquake, *Science* **345,** no. 6201, 1165–1169, doi: 10.1126/science.1256074.
Udías, A., R. Madariaga, E. Buforn, D. Muñoz, and M. Ros (2012). The large Chilean historical earthquakes of 1647, 1657, 1730, and 1751 from contemporary documents, *Bull. Seismol. Soc. Am.* **102,** 1639–1653.
Urrutia, R., and C. Lanza (1993). *Catástrofes en Chile 1541–1992*, Editorial la Noria, Santiago, Chile.
VanDecar, J. C., and R. S. Crosson (1990). Determination of teleseismic relative phase arrival times using multi-channel cross-correlation and least squares, *Bull. Seismol. Soc. Am.* **80,** 150–169.
Vargas, G., M. Farías, S. Carretier, A. Tassara, S. Baize, and D. Melnick (2011). Coastal uplift and tsunami effects associated to the 2010 M_w 8.8 Maule earthquake in central Chile, *Andean Geol.* **38,** no. 1, 219–238.
Vigny, C., A. Rudloff, J. C. Ruegg, R. Madariaga, J. Campos, and M. Alvarez (2009). Upper plate deformation measured by GPS in the Coquimbo Gap, Chile, *Phys. Earth Planet. Inter.* **175,** nos. 1/2, 86–95.
Vigny, C., A. Socquet, S. Peyrat, J. C. Ruegg, M. Métois, R. Madariaga, S. Morvan, M. Lancieri, R. Lacassin, J. Campos, *et al.* (2011). The 2010 (M_w 8.8) Maule megathrust earthquake of central Chile, monitored by GPS, *Science* **332,** 1417–1421.
Watanabe, S, M. Sato, M. Fujita, T. Ishikawa, Y. Yokota, N. Ujihara, and A. Asada (2014). Evidence of viscoelastic deformation following the 2011 Tohoku-Oki earthquake revealed from seafloor geodetic observation, *Geophys. Res. Lett.* **41,** no. 16, 5789–5796, doi: 10.1002/2014GL061134.

Sergio Ruiz
Departamento de Geofísica
Universidad de Chile
Blanco Encalada 2002
Santiago, Chile
sruiz@dgf.uchile.cl

Emilie Klein
Vigny Christophe
Raúl Madariaga
Luce Fleitout
Laboratoire de Géologie
École Normale Supérieure
24 Rue Lhomond
75231 Paris, France

Francisco del Campo
Juan Carlos Baez
Felipe Leyton
Centro Sismologico Nacional
Universidad de Chile
Blanco Encalada 2002
Santiago, Chile

Efrain Rivera
Gabriel Vargas
Departamento de Geología
Universidad de Chile
Plaza Ercilla 803
Santiago, Chile

Piero Poli
Massachusetts Institute of Technology
77 Massachusetts Avenue
Cambridge, Massachusetts 02139 U.S.A.

Marianne Metois
Laboratoire de Geologie de Lyon
Terre, Planetes, Environnement
Universite de Lyon
CNRS UMR5276, Universite Lyon 1 - ENS Lyon
Villeurbanne, France

Published Online 25 May 2016